

RIGA TECHNICAL UNIVERSITY
Faculty of Materials Science and Applied Chemistry
Institute of General Chemical Engineering

Kristaps RUBENIS
Student of the Doctoral study programme „Materials Science”

**OBTAINING OF TIN DIOXIDE BASED MATERIALS,
CHARACTERIZATION OF STRUCTURE AND PHYSICAL
PROPERTIES**

Summary of the Doctoral Thesis

Doctoral advisor
Dr.sc.ing., docent
D. LOČA

RTU Press
Riga 2017

Rubenis K. Obtaining of tin dioxide based materials, characterization of structure and physical properties. – R.: RTU Press, 2017. – 30 pages.

Printed in accordance to decision of Institute of General Chemical Engineering on June 16th, 2016, protocol No. 15-15/16

ISBN 978-9934-10-949-2

**THE DOCTORAL THESIS PROPOSED TO RIGA TECHNICAL
UNIVERSITY FOR THE PROMOTION TO THE SCIENTIFIC DEGREE
OF DOCTOR OF ENGINEERING SCIENCES**

To be granted the scientific degree of Doctor of Engineering Sciences, the Doctoral Thesis will be defended on 31 May 2017 at the Faculty of Materials Science and Applied Chemistry of Riga Technical University, 3 Paula Valdena Street, Room 272.

OFFICIAL REVIEWERS

Professor, *Dr.habil.sc.ing.* Jānis Grabis
Institute of Inorganic Chemistry, Riga Technical University, Latvia

Leading researcher, *Dr. phys.* Anatolijs Šarakovskis
Institute of Solid State Physics, University of Latvia, Latvia

Dr. Krzysztof Galazka
Institute of Plasma Physics and Laser Microfusion, Poland

DECLARATION OF ACADEMIC INTEGRITY

I hereby confirm that the present Doctoral Thesis submitted for the review to the Riga Technical University for the promotion to the scientific degree of Doctor of Engineering Sciences is my own work. The Thesis has not been submitted to any other university for the promotion to any other degree.

Kristaps Rubenis

Date:

The Doctoral Thesis is written in Latvian language. The volume of the Doctoral Thesis is 121 pages and it contains 55 illustrations, 11 tables, 36 equations and 156 literature references.

ACKNOWLEDGEMENT

I wish to express my sincere gratitude to my thesis advisor, Dagnija Loča, for her advice, trust, motivation and objective criticism throughout all stages of this dissertation. I would like to thank Jānis Ločs for his support, consultations, and ideas he provided for conducting the experiments. My gratitude is also extended to Professor Līga Bērziņa-Cimdiņa, who accepted me to be a part of the Institute of General Chemical Engineering.

I would like to thank the collective of the Institute of General Chemical Engineering, which has always supported me throughout the process of writing this thesis. My special thanks are to Agnese Pūra.

My thanks are also due to the employees of RTU Department of Electronics Equipment Valdis Teteris and Jānis Barloti, for their support and advice especially during the initial stage of this dissertation.

I would like to give my special thanks to *Dr. Sascha Populoh* who was my mentor during my stay at Swiss Federal Laboratories for Materials Science and Technology (Switzerland) in the scope of the Latvian-Swiss Cooperation Programme for higher education and science. I would also like to thank *Dr. Philipp Thiel*, *Dr. Songhal Yoon* and *Dr. Corsin Battaglia*.

Finally, I express the most wholehearted gratitude to my family and especially my wife Līga, for their support and tolerance throughout all stages of this dissertation.

TABLE OF CONTENTS

General overview of the thesis	6
Introduction	6
Aim.....	6
Tasks.....	6
Scientific importance and novelty	7
Practical importance	7
Thesis statements to be defended	7
Author's contribution	7
Author's publications and participation in conferences	7
Literature review	8
Experimental section	9
Hydrothermal synthesis of SnO ₂ , characterization of the obtained materials.....	9
Spark plasma sintering of SnO ₂ and Sb-doped SnO ₂ synthesized by chemical co-precipitation method, characterization of the obtained samples	10
Main results of the thesis.....	11
1.1. Synthesis of SnO ₂ by hydrothermal method, characterization of the synthesized materials	11
Effect of NaOH/HCl addition to the synthesis starting solution on the structure and gas sensing properties of the synthesized SnO ₂	11
2.1. Obtaining of SnO ₂ and Sb doped SnO ₂ ceramics by spark plasma sintering method, characterization of the obtained materials.....	19
Characterization of SnO ₂ and Sb doped SnO ₂ prepared by co-precipitation method	19
Sintering of SnO ₂ and Sb doped SnO ₂ by spark plasma sintering method.....	20
Characterization of the spark plasma sintered Sn _{1-x} Sb _x O ₂ samples	20
Characterization of the post-spark plasma sintering annealed Sn _{1-x} Sb _x O ₂ samples	23
Conclusions	28
Literature references.....	29
Author's publications and participation in conferences.....	30

GENERAL OVERVIEW OF THE THESIS

Introduction

Thanks to its unique chemical and physical properties, tin dioxide is one of the most widely used semiconducting oxides. For example, it is the most commonly used chemoresistor in chemoresistive gas sensors whose principle of operation is based on the interaction of the gas molecules being detected with the oxygen ionosorbed on the surface of the chemoresistive material.

Nowadays the trend of miniaturization has affected the field of gas sensors as well, since, for example, the energy (elevated temperature) required for sensor operation can be decreased by reducing the sensor dimensions. During the last decades, the use of nanostructured chemoresistive materials has become increasingly popular, since they have better gas sensing properties compared to the respective micron-sized materials. The use of different 2D and 3D nano/micro structures has become especially popular, since they agglomerate less compared to nanoparticles and, as a result, the gas molecules can diffuse more freely into the volume of chemoresistive material layer, providing higher sensitivity and shorter response time. One of the synthesis methods that can be used to produce nanostructured materials with various sizes and shapes is hydro/solvothermal synthesis method. The size and shape of the hydro/solvothermally synthesized material and its properties strongly depends on the composition of the synthesis starting solution, temperature and time. Although during the last few years there are many scientific articles published on a synthesis of novel chemoresistive materials and improvement of existing ones by using hydro/solvothermal synthesis method, there is still possibilities to develop them further, for example, by modifying the previously mentioned synthesis parameters.

Additionally SnO₂ and SnO₂ based materials lately find applications in areas where they previously weren't used. For example, some studies show that SnO₂ could have certain perspectives in the field of oxide based thermoelectric materials, however, for practical application thermal conductivity of the material should be greatly reduced as well as in the context of ceramic materials, improvement of material's density is necessary.

Aim

To clarify how different hydrothermal synthesis parameters affect structural and gas sensing properties of SnO₂, as well as to find out the effect of spark plasma sintering on SnO₂ and Sb (1–5 mole%) doped SnO₂ structural and thermoelectrical properties.

Tasks

1. Summarize the information available in scientific literature on SnO₂ gas sensing and thermoelectric properties and their affecting factors, synthesis methods of SnO₂ including hydrothermal synthesis method, as well as sintering of SnO₂;
2. By varying the hydrothermal synthesis parameters (composition of the synthesis starting solution, time and temperature) synthesize SnO₂;
3. Characterize the structural and gas sensing properties of SnO₂ obtained by hydrothermal synthesis method;
4. Obtain dense (>90 % of theoretical densit) SnO₂ un ar Sb (1–5 mole %) doped SnO₂ ceramics samples by spark plasma sintering method, perform annealing of the obtained samples in air;
5. Characterize structural and thermoelectric properties of the spark plasma sintered SnO₂ and Sb doped SnO₂ samples before and after annealing in air.

Scientific importance and novelty

Effect of several relatively little investigated hydrothermal synthesis parameters (like, other co-solvents except ethanol) on structural and gas sensing properties of SnO₂ have been investigated. Additionally, for the first time to the author's knowledge the effect of spark plasma sintering on SnO₂ and Sb (1–5 mole %) doped SnO₂ thermoelectric properties (including thermal conductivity and thermoelectric figure of merit) was investigated.

Practical importance

The obtained and characterized materials potentially can be used in chemoresistive gas sensors as well as in the field of thermoelectric power generation.

Thesis statements to be defended

1. It is possible to increase/decrease specific surface area and decrease/increase crystallite size of the synthesized SnO₂, by changing the type of alcohol added to the hydrothermal synthesis starting solution to the one with longer chain of carbon atoms and vice versa from the row methanol>ethanol>isopropanol;
2. Thermoelectric power factor of Sb (1–5 mole%) doped SnO₂ ceramics obtained by spark plasma sintering method can be improved by annealing under air – the increase in electrical conductivity (due to the oxidation of Sb³⁺ to Sb⁵⁺) compensates the decrease of Seebeck coefficient.

Author's contribution

Synthesis, sintering by spark plasma sintering method, measurements of density, differential scanning calorimetry, differential thermal analysis/thermogravimetry, characterization of crystal structure (X-ray diffraction), morphology (scanning electron microscopy), thermal diffusivity, Seebeck coefficient, electrical resistivity and gas sensing properties of all samples, as well as processing and interpretation of the obtained results is done by author.

Raman spectroscopy was done by *M. Sc.* Andrii Voznyi (Riga Technical University, Sumy State University, Ukraine), Fourier transformation infrared spectroscopy was done by *Dr. sc. ing.* Līga Stīpniece (Riga Technical University), N₂ sorbtometry was done by *Mg. sc. ing.* Valentīna Stepanova (Riga Technical University) while X-ray photoelectron spectroscopy for the samples was done by *Dr.* Ulrich Müller (Swiss Federal Laboratories for Materials Science and Technology, Switzerland).

Author's publications and participation in conferences

3 scientific articles relevant to dissertation and 2 not related have been published during the PhD studies. Additionally, participation in 8 scientific conferences has been taken.

LITERATURE REVIEW

Literature review of the thesis contains information on properties (including gas sensing and thermoelectric properties) and applications of SnO₂, synthesis methods of nanostructured materials, chemoresistive materials and factors affecting their properties, thermoelectric effects and methods to improve thermoelectric properties of the material, as well as sintering processes and methods used for sintering of difficult to sinter materials (like SnO₂).

Scientific literature contains many articles dedicated to characterization of SnO₂ and SnO₂ based materials as well as to improvement of their properties, mainly focusing on the main SnO₂ applications – transparent conductive coatings, oxidation catalysts and chemoresistive gas sensors. Thanks to its unique chemical and physical properties, SnO₂, is one of the most widely used materials in chemoresistive gas sensors, whose principle of operation is based on the interaction of the gas molecules being detected with the ionosorbed oxygen on the surface of the chemoresistive material (like SnO₂). To improve gas sensing properties of SnO₂, it can be doped with various chemical elements as well as combined with other materials. Gas sensing properties of SnO₂ can be improved by nanostructuring approach as well. Since the principle of chemoresistive gas sensors operation is directly based on the processes that occurs on the surface of the chemoresistive material, the decrease in particle size and the respective increase in specific surface area of the material improves its gas sensing properties. During the last decade great attention has been paid to the synthesis of different 2D and 3D as well as hierarchical nanostructures of SnO₂ for the applications in chemoresistive gas sensors. The respective structures are less agglomerated compared to nanoparticles and as a result the gas molecules can more freely diffuse into the volume of the chemoresistive material layer deposited onto the substrate, providing higher sensitivity and shorter response time. Additionally, due to the fact that specific crystal planes can differently interact with atmospheric oxygen and molecules of different gases, the nanostructures where growth of certain crystal planes are realised over others can improve gas sensing properties of the material as well. One of the synthesis methods that can be used to produce nanostructured materials with various shapes and is gaining great attention lately is hydro/solvothermal synthesis method. Hydro/solvothermal synthesis is a process during which the crystallization of necessary compounds occurs in a water or other solvent media at high vapour pressure. Under laboratory conditions that can be realized in a simple hydrothermal synthesis reactor. Many studies have been dedicated to synthesis of specific SnO₂ nanostructures by hydro/solvothermal synthesis method, however, in most cases the effect of synthesis parameters (for example, composition of the hydro/solvothermal synthesis starting solution, effect of co-solvents, synthesis temperature and time) on the obtained material structure and dependant properties are not evaluated.

Lately SnO₂ and SnO₂ based materials finds applications in areas where they previously weren't used. For example, SnO₂ is considered as a perspective material (anode) for applications in the new generation Li-ion batteries and supercapacitators [1]. Some studies shows that SnO₂ could have certain perspectives in the field of oxide based thermoelectric materials as well [2], [3]. Information of undoped as well as doped SnO₂ thermoelectric properties can be found in the scientific literature, characterized for thin films as well as bulk materials – ceramics and monocrystals, however, relatively little studies have been devoted to this topic. In the case of ceramic materials this can be attributed to samples density, because dense SnO₂ ceramics can't be obtained by traditional sintering method, while the use of sintering additives unfavorably affect thermoelectric properties of SnO₂. Additionally, SnO₂ have high thermal conductivity (~40 W/m·K), that should be greatly decreased for the material's application in the field of thermoelectrics. In order to improve electrical conductivity and thermoelectric properties of SnO₂, it is usually doped with Sb. Dense SnO₂ and Sb doped SnO₂ ceramics with high electrical conductivity (>2·10³ S/m) without the use of sintering additives can be obtained by hot-pressing methods. The pressure applied to the sample during

the sintering process improves diffusion processes in to the lattice and grain boundaries and allows to obtain dense samples ($\rho > 95\%$ of theoretical material density). Additionally, the fast heating and cooling rate that can be realized if spark plasma sintering method (SPS) is used, allows to obtain nanostructured materials that could have reduced thermal conductivity and therefore improved thermoelectric properties. However, there are practically no studies done on characterization of thermoelectric properties of SnO₂ and Sb doped SnO₂ obtained by SPS method.

EXPERIMENTAL SECTION

Hydrothermal synthesis of SnO₂, characterization of the obtained materials

The principal synthesis of SnO₂ by hydrothermal method was done as follows: 1 g (0.00285 mole) of SnCl₄·5H₂O was added to 60 ml of deionized water (if synthesis was done in the H₂O/co-solvent media, 30 ml of H₂O and 30 ml of the respective co-solvent was used) under vigorous magnetic stirring (500 rpm). After ½ h, a certain amount (0; 0.0125; 0.0250 vai 0.0375 mole) NaOH or HCl (attributed to absolute HCl) was added to the previously prepared SnCl₄·5H₂O solution under continuous stirring. Afterward, the obtained solution was transferred to a Teflon-lined hydrothermal synthesis reactor, that after closing was placed into the drying oven and exposed to a predetermined heating (5 K/min), isothermal holding (393–473 K; 1–24 h) and cooling (5 K/min) regime. The precipitates obtained at the end of the hydrothermal synthesis was separated from the liquid phase by centrifugation (2420 RCF), afterward several times rinsed with deionized water and ethanol, and finally dried at 353 K for 24h in a drying oven.

To clarify the effect of thermal treatment on dimensional stability and gas sensing properties of the hydrothermally synthesized material, part of the obtained SnO₂ was thermally treated under air at 673 K for 3 h.

Crystal structure (X-ray diffraction method), surface morphology (scanning electron microscopy) and specific surface area (BET method) of the obtained materials were characterized. Additionally, Fourier transformation infrared spectroscopy and Raman spectroscopy were performed on the samples, as well as their gas sensing against 100 ppm ethanol vapor in the air were characterized.

For characterization of the gas sensing properties, the synthesized material was mixed with a small amount of ethanol by using ultrasonic horn, until viscous, homogeneous paste was obtained. Afterward, the obtained paste with an assist of micro spatula was coated onto a previously prepared sensor substrate – Al₂O₃ tube (Ni-Cr heating element inserted into a tube) with a pair of electrodes. The gas sensing measurements were performed under static conditions (inside the hermetic container where sensor element was inserted/removed by using a sluice-type valve. Gas sensitivity of the samples was characterised versus a certain concentration of ethanol vapour in air, that was achieved inside the container by introducing a certain amount of ethanol in the liquid phase and allowing to evaporate (a small fan mounted inside the container was used to increase the evaporation rate of ethanol, but wasn't operated during the measurement). A voltage divider principle was used to detect changes in electrical resistivity of the sensor (sample), that were caused by the insertation/removal of the sensor element in/from the gas medium. The electrical resistivity of the sensor in the air and in the gas media was calculated by using equation 1.1., using the voltage values measured on the load resistor by a digital multimeter.

$$R_{sensor} = \left(\frac{U_{circuit} - U_{output}}{U_{output}} \right) \cdot R_{load} \quad (1.1.)$$

Gas sensing of the samples was determined in the temperature range of 423 to 673 K (substrate temperature). Gas sensing of the samples was calculated by using equation 1.2.

$$S = \frac{R_{air}}{R_{gas}}, \quad (1.2.)$$

where S – response of sensor (sample);

R_{air} – electrical resistivity of the sensor (sample) before insertation in the gas media (chamber);

R_{gas} – saturation value of electrical resistivity of the sensor in gas media.

The room temperature during the measurements was 295 ± 2 K, relative humidity: 50–60 %.

Spark plasma sintering of SnO₂ and Sb-doped SnO₂ synthesized by chemical co-precipitation method, characterization of the obtained samples

Depending on the obtainable Sn_{1-x}Sb_xO₂ ($x = 0; 0.01; 0.03; 0.05$) composition, to a 1 M SnCl₄·5H₂O solution in water a certain amount of SbCl₃ was added (as 20 % w/w solution in concentrated HCl) under vigorous magnetic stirring (500 rpm). After ½ h, to a SnCl₄·5H₂O and SbCl₃ containing solution 1 M aqueous NH₃ solution was added drop wise under continuous vigorous stirring, until pH = 4 was reached. The obtained suspensions were left to stand for 24 h, then were filtered and washed with highly purified water, dried at 373 K for 24h and finally calcined at 773 K for 3 h (heating/cooling rate: 2 K/min). The calcined materials were afterwards ground into fine powders by using mortar and pestle.

The Sn_{1-x}Sb_xO₂ powders obtained by thermal treatment of the solid products obtained by chemical co-precipitation method were sintered by the spark plasma sintering (SPS) method. Graphite die was used to obtain pellet shaped samples. In order to protect the die from direct contact with the Sn_{1-x}Sb_xO₂ powders, the surfaces of the die which comes in a direct contact with the powder were covered with a graphite foil. For preparation of each sample, approximately 2 g of the respective Sn_{1-x}Sb_xO₂ composition powder was used. During all of the SPS process, the samples were exposed to a 50 MPa of uniaxial pressure. The sintering was done under argon atmosphere. During the SPS process, the samples were heated with a rate of 100 K/min, however, before they reached the isothermal holding (sintering) temperature, the heating rate was decreased to 25 K/min, in order to prevent overrunning of the pre-determined isothermal holding temperature. The time of isothermal holding stage for all samples was 3 min. After the end of the isothermal holding stage the sample containing die was allowed to naturally cool to room temperature. After the end of the SPS process the samples were removed from the die and grinded/polished till completely cleaned from the graphite foil.

In order to improve electrical conductivity of the Sn_{1-x}Sb_xO₂ samples obtained by SPS, they were annealed under air. The annealing was done at three different temperatures: 1073, 1173 and 1248 K (holding time: 48 h, heating/cooling rate: 2 K/min).

Crystal structure (X-ray diffraction method), surface morphology (scanning electron microscopy) and specific surface area (BET method) of the SnO₂ and Sb doped SnO₂ powders obtained by chemical co-precipitation method were characterized.

Crystal structure (X-ray diffraction method), fracture surface morphology (scanning electron microscopy), density (Archimed's method) was characterized for the SPSed and post-SPS annealed SnO₂ and Sb doped SnO₂ samples as well as chemical composition and chemical bounding character of the respective samples were characterized (X-ray photoelectron spectroscopy). Additionally, thermoelectric properties of the samples were characterized in the temperature range of T_{room} to 1073 K. Seebeck coefficient as well as electrical conductivity of the samples were determined by using a commercial equipment *RZ200li* (Ozawa science, Japan). The measurements were done on rectangular shaped samples cut from the sintered/annealed pellets with a high precision saw. Electrical conductivity of the samples was determined by a 4-point method, while Seebeck coefficient was determined by a steady state method. Thermal conductivity of the samples was calculated by using the predetermined values of sample's density, thermal diffusivity and heat capacity. Thermoelectric figure of merit of the samples was calculated by using equation 1.3.

$$Z(T) = \frac{S^2 \sigma}{k} \cdot T, \quad (1.3.)$$

where S – Seebeck coefficient of the sample;
 σ – electrical conductivity of the sample;
 k – thermal conductivity of the sample.

MAIN RESULTS OF THE THESIS

1.1. Synthesis of SnO₂ by hydrothermal method, characterization of the synthesized materials

Effect of NaOH/HCl addition to the synthesis starting solution on the structure and gas sensing properties of the synthesized SnO₂

X-ray diffraction patterns of the solid products obtained by hydrothermal synthesis (done at 473 K temperature for 12 h) from starting solutions containing 1 gr of (0.0285 mol) SnCl₄·5H₂O and a certain amount (0; 0.0125; 0.0250 or 0.0375 mol) of NaOH or HCl (attributed to absolute HCl) dissolved in 60 ml of water can be seen in Fig. 1.

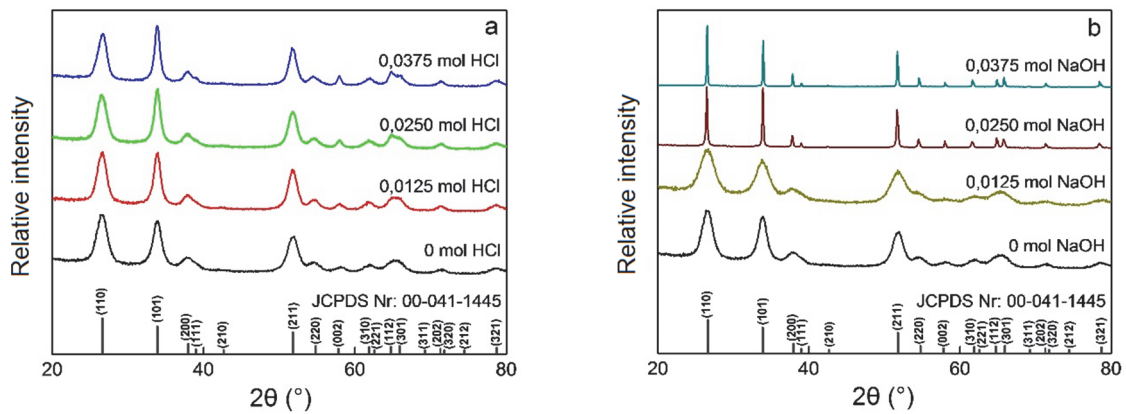


Fig.1. X-ray diffraction patterns of the solid products obtained by hydrothermal synthesis depending on the amount of HCl (a) or NaOH (b) added to synthesis starting solution.

All diffraction reflexes detected in the X-ray diffraction patterns (Fig. 1.) of the solid products obtained by hydrothermal synthesis were identified as corresponding to the cassiterite phase of SnO₂ (ICDD card No. 00-041-1445), however, differences in their relative intensities and full-width at half-maximums (FWHM) can be observed depending on the amount of HCl or NaOH added to synthesis starting solution.

Additionally, the amount of HCl or NaOH used affect specific surface area (SSA) and crystallite size of the synthesized materials (Table 1). Drastic reduction in the SSA and increase in crystallite size of the obtained material can be observed when 0.0250 or 0.0375 mol NaOH is added to the synthesis starting solution.

Table 1

The SSA, FWHM of the diffraction reflexes and average crystallite size of the SnO₂ obtained by hydrothermal synthesis method depending on the amount of HCl or NaOH added to SnO₂ synthesis starting solution

Amount of HCl or NaOH in the synthesis starting solution	SSA (m ² /g)	FWHM of diffraction reflex 110 ((°) 2θ)	Average crystallite size (nm)
0.0375 mol HCl	84.5	1.30	6.5
0.0250 mol HCl	87.8	1.45	6.1
0.0125 ml HCl	84.0	1.42	6.2
0 mol HCl/NaOH	116.9	1.61	5.4
0.0125 mol NaOH	149.1	1.90	4.6
0.0250 mol NaOH	1.4	0.18	>100
0.0375 mol NaOH	8.2	0.15	>100

The synthesized material consists of nanoparticles in cases when the synthesis starting solution contained only SnCl₄·5H₂O or additionally to that also 0.0125–0.0375 mol HCl or 0.0125 mol NaOH (Fig. 2.). Hierarchical SnO₂ structures (with dimensions in the micron range) which consists of interconnected sphere-like rod clusters that radially grows from a common center forms when 0.0250 mol NaOH was added to the synthesis starting solution. The presence of rod-like crystal structures to the aforementioned hierarchical structures can be observed if 0.0375 mol NaOH was added to the synthesis starting solution.

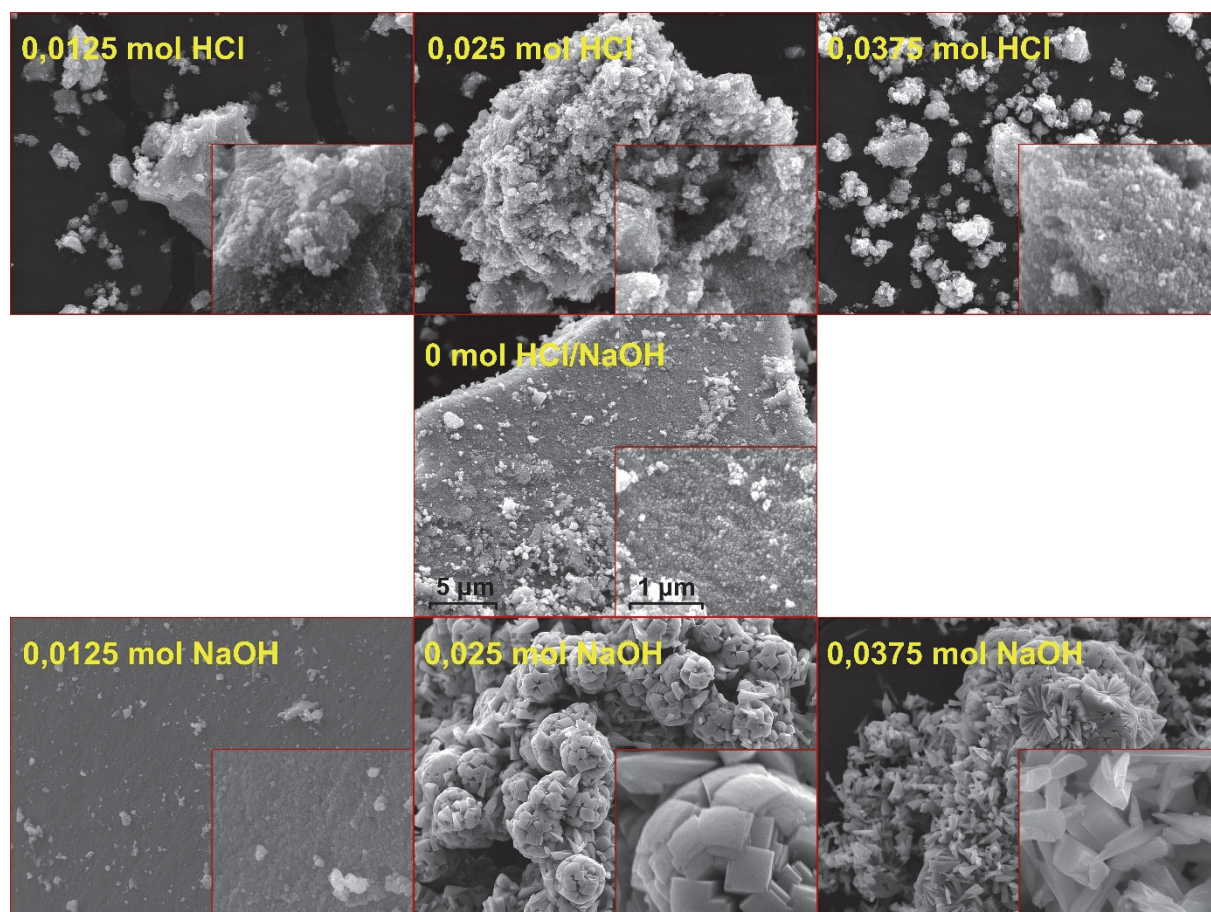
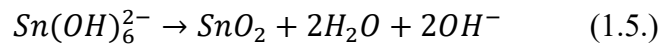
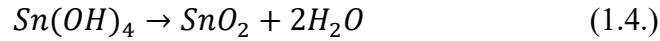


Fig.2. Surface morphology (SEM) of the hydrothermally synthesized SnO₂, depending on the amount of HCl or NaOH added to the synthesis starting solution.

Condensation reactions in acidic and neutral media (can be attributed to the cases when 0.0125–0.0375 mol HCl or 0.0125 mol of NaOH was used) occurs faster than in basic media and as a result, relatively large amount of nucleation centers can form under these conditions, favoring the formation of nanoparticles [4].

During the initial stage of the hydrothermal synthesis in basic media (when relative concentration of Sn^{4+} to OH^- ions is the synthesis solution is high) SnO_2 can form according to the principle shown in equation 1.4. SnO_2 particles that forms because of $\text{Sn}(\text{OH})_4$ dehydration can act as nucleation centers for further crystal growth. When concentration of Sn^{4+} in the solution decreases and OH^- starts to predominate, formation of $\text{Sn}(\text{OH})_6^{2-}$ becomes possible from which SnO_2 can form according to the principle shown in equation 1.5. In this case, growth of crystals instead of formation of new crystallization centers is favoured.



As can be expected, higher sensitivity towards the ethanol vapour concentration of 100 ppm (Fig. 3.) shows the synthesized SnO_2 with crystallite size <7 nm (Table 1). The highest $R_{\text{air}}/R_{\text{gas}}$ value of ~ 50 at 473 K shows the sample whose synthesis starting solution contained 0.0125 moles of NaOH. The sensitivity of other samples made of nanosized crystallites are in the range of 37 to 43. The hierarchical SnO_2 structures (samples whose synthesis starting solution contained 0.0250 or 0.0375 mol NaOH) have substantially lower sensitivity. The highest sensitivity (8 – the sample whose synthesis starting solution contained 0.0250 mol NaOH and 11 – the sample whose synthesis starting solution contained 0.0375 mol NaOH), respective samples shows at 523 K temperature.

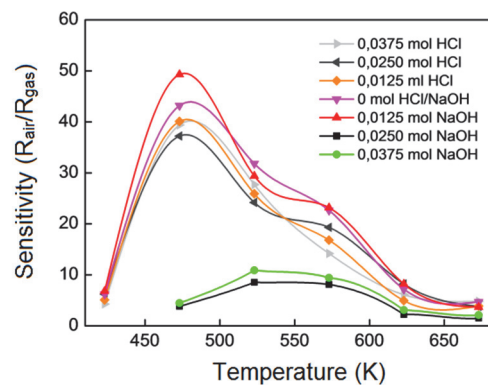


Fig.3. Ethanol (100 ppm) sensitivity of the hydrothermally synthesized SnO_2 as a function of temperature, depending on the amount of HCl or NaOH added to SnO_2 synthesis starting solution.

Higher sensitivity of the nanostructured samples compared to the hierarchical ones are attributable to their relatively thicker space-charge layer formed by oxygen ionosorbption on the surface of SnO_2 due to smaller crystallite size [5].

To assess dimensional stability of the synthesized materials at elevated temperatures, they were thermally treated in air at 673 K for 3h. Specific surface area of the synthesized SnO_2 with crystallite size <7 nm (Table 1) after thermal treatment, depending on the amount of HCl/NaOH added to its synthesis starting solution, decreases by 39–59 % while crystallite size increases by 38–44 % (Table 2).

Table 2

The SSA, FWHM of the diffraction reflexes and average crystallite size of the heat treated (673 K for 3 h) SnO₂ obtained by hydrothermal synthesis method, depending on the amount of HCl or NaOH added to SnO₂ synthesis starting solution

Amount of HCl or NaOH in the synthesis starting solution	SSA (m ² /g)	FWHM of diffraction reflex 110 ((°) 2θ)	Average crystallite size (nm)
0.0375 mol HCl	52.0	0.84	11.0
0.0250 mol HCl	53.7	0.88	10.4
0.0125 ml HCl	61.6	1.06	8.6
0 mol HCl/NaOH	57.7	1.15	7.8
0.0125 mol NaOH	62.1	1.21	7.5
0.0250 mol NaOH	2.0	0.17	>100
0.0375 mol NaOH	–	0.15	>100

As expected, the structural changes caused by thermal treatment of the synthesized materials greatly affect their gas sensitivity (see Fig. 4.). Sensitivity towards the ethanol vapour concentration of 100 ppm at 473 K for the synthesized SnO₂ with crystallite size <7 nm (Table 1) after annealing decreases by 49–51 % and are 18 to 25 (depending on the amount of HCl/NaOH added to their synthesis starting solution). Decrease in sensitivity of the hierarchical SnO₂ structures (samples whose synthesis starting solution contained 0.0250 or 0.0375 mol NaOH) after thermal treatment can be observed as well.

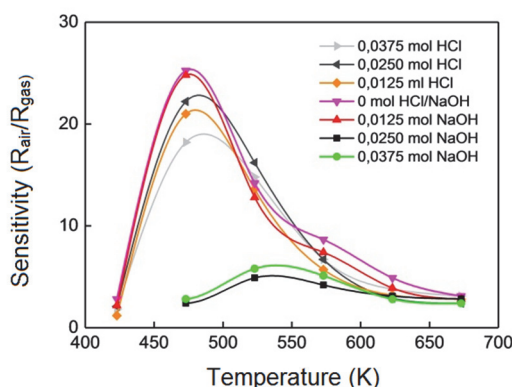


Fig.4. Ethanol (100 ppm) sensitivity of the hydrothermally synthesized SnO₂ after heat treatment at 673 K for 3h as a function of temperature, depending on the amount of HCl or NaOH added to SnO₂ synthesis starting solution.

The observed changes in sensitivity after thermal treatment of the synthesized materials can be attributed to decrease in space-charge layer thickness due to increase in crystallite size as well as to the changes in quantity of surface defects [6].

Effect of co-solvent addition to the hydrothermal synthesis starting solution on structure and gas sensing properties of SnO₂

Ethanol is the most commonly added co-solvent to the hydrothermal synthesis starting solution of SnO₂ to modify morphology of the material. In the present study, the effect of various other alcoholic co-solvents besides ethanol (methanol, ethanol, 2-propanol, ethylene glycol and glycerol) on the formation of SnO₂ during the hydrothermal synthesis was investigated. In this study, the synthesis media consisted of 30 ml of water and 30 ml of the respective co-solvent (or 60 ml of water if co-solvent was not used) where 1g of SnCl₄·5H₂O and 1g of NaOH were dissolved. In all cases the synthesis was done at 473 K for 12 h.

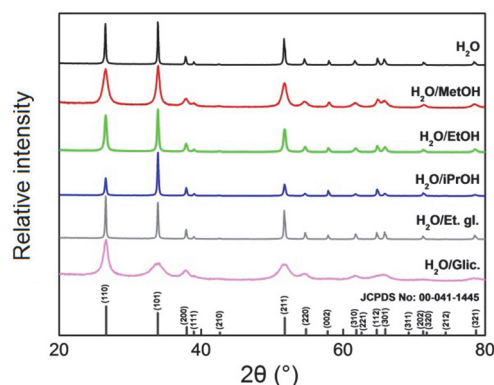


Fig. 5. X-ray diffraction patterns of the hydrothermally synthesized solid products depending on the synthesis medium used.

All of the detected diffraction reflexes in the recorded diffraction patterns (Fig. 5.) for all of the synthesized products regardless of whether the co-solvent was used or not can be attributed to the tetragonal cassiterite phase of SnO_2 (JCPDS card No. 00-041-1554). However, shape and intensity of the reflexes changes depending on the synthesis media used.

As can be seen from Fig. 6, the use of the respective co-solvents greatly affect morphological evolution of SnO_2 . As mentioned before, without the use of co-solvent the synthesized material mainly consists of interconnected micron sized sphere-like rod clusters that radially grows from a common center. The obtained material mainly consists of agglomerated nanoparticle clusters, if methanol was used as a co-solvent, however, some regions with nanosized rod-like structures can be observed as well. Rod-cluster structures are formed when ethanol or 2-propanol co-solvents were used, though the diameter of the rods is smaller as well as they are arranged in a different fashion compared to the case when synthesis was done in the aqueous media. In the case of ethanol co-solvent the rods are mainly assembled in a flower-like structures while twin-layered rod arrays are mainly formed if 2-propanol is used as a co-solvent. Furthermore, it can be observed that diameter of the rods is larger if 2-propanol instead of ethanol was used. Spherical aggregates of thin semicircular sheets are formed if ethylene glycol co-solvent was used while dense micron sized spheres with roughened surface are formed in the case of glycerol co-solvent.

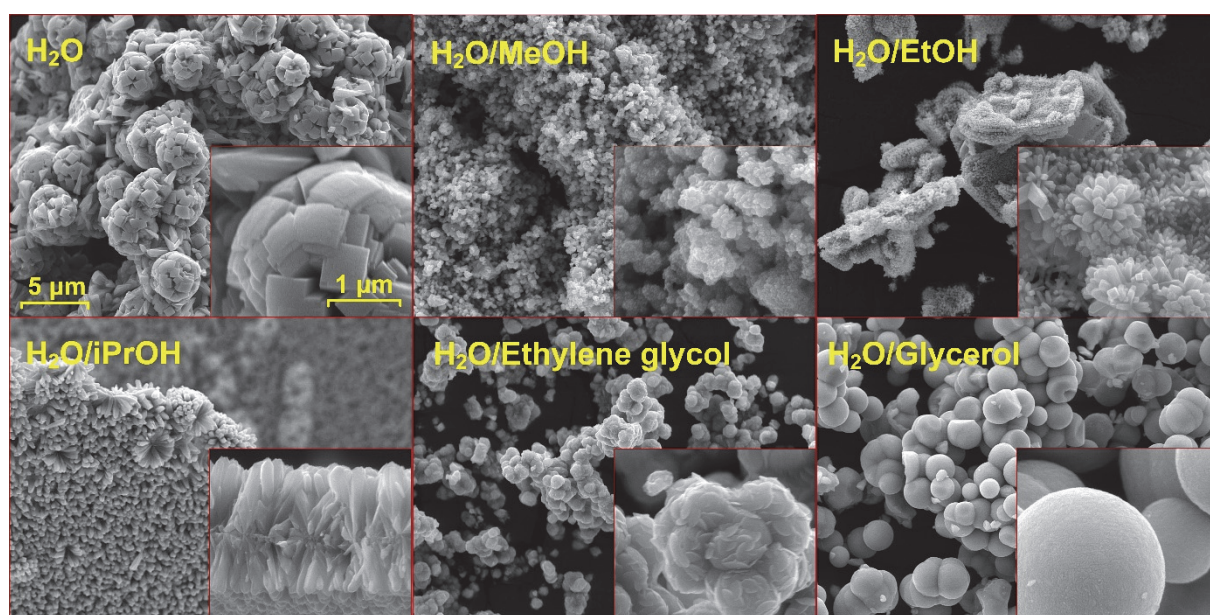


Fig.6. SEM micrographs of the hydrothermally synthesized SnO_2 structures depending on the medium used for the synthesis.

The SSA of the synthesized material varies greatly depending on the synthesis media used (Table 3). Independently of the co-solvent type the SSA of the synthesized material is larger in all cases when synthesis was done in the presence of co-solvent. The SnO₂ synthesized in the water/MeOH media have the largest SSA (10.9 m²/g). If short-carbon-chain alcoholic co-solvents are used (methanol, ethanol, 2-propanol), the SSA of the synthesized material decreases with an increasing number of carbon atoms in the alcohol molecule.

Table 3

The SSA, FWHM of the diffraction reflexes and average crystallite size of the synthesized SnO₂, depending on the synthesis medium used

Synthesis media	SSA _{BET} (m ² /g) of the synthesized material	FWHM of diffraction reflex 110 ((°) 2θ)	Average crystallite size (nm)
H ₂ O	1.4	0.18	>100
H ₂ O/MeOH	10.9	0.8	12
H ₂ O/EtOH	2.8	0.34	34
H ₂ O/iPrOH	1.5	0.22	70
H ₂ O/Ethylene glycol	6.1	0.17	>100
H ₂ O/Glycerol	5.7	0.78	12

The observed differences in the crystal structure, morphology and SSA of the synthesized SnO₂ depending on the synthesis media used can be attributed to various factors. For example, the used co-solvents differently affect the solubility of the starting reactants (SnCl₄ · 5H₂O and NaOH) as well as their reaction products (for example, Na₂Sn(OH)₆). Additionally, they have different viscosities as compared with water and to each other and, therefore, their presence can change the viscosity of the synthesis media, thus altering diffusion processes and growth rate of SnO₂ crystals. Since the used co-solvents have different vapor pressures, the pressure inside the reaction vessel changes if synthesis is done in the presence of co-solvent, affecting diffusion processes as well. Adsorption of the co-solvent molecules on certain crystal faces, as a result inhibiting crystal growth in certain directions, is also possible.

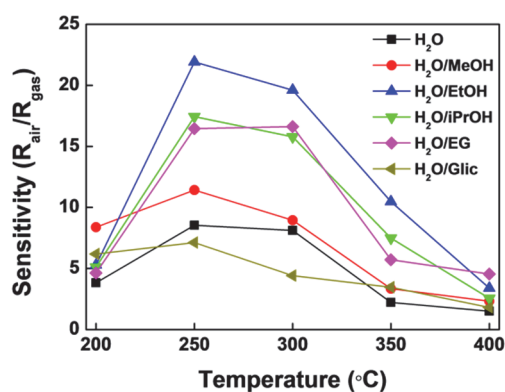


Fig.7. Ethanol (100 ppm) sensitivity of the hydrothermally synthesized SnO₂ structures, depending on the medium used for SnO₂ synthesis.

Even though the SnO₂ synthesized in the H₂O/MeOH media have the largest SSA among all the samples, the highest sensitivity ~22 towards the ethanol vapour concentration of 100 ppm at 523 K temperature shows the sample synthesized in the presence of ethanol co-solvent.

To determine the possible reasons for the respective observations, FT-IR and Raman spectra of the synthesized samples were recorded.

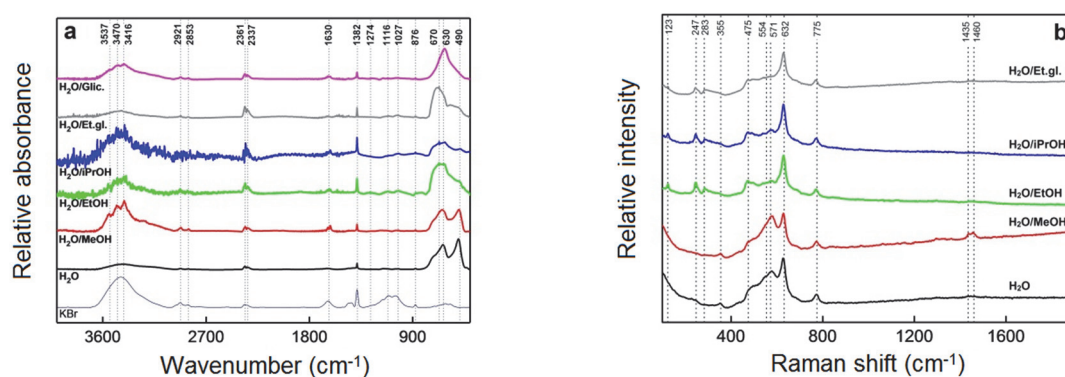


Fig.8. FT-IR (a) and Raman (b) spectrum of the hydrothermally synthesized SnO₂, depending on the medium used for SnO₂ synthesis.

Great differences depending on the used co-solvent type can be observed in the characteristic region of SnO₂ absorption bands ($<800\text{ cm}^{-1}$). Overlap of similar intensities absorption bands with maximums at 630 and 490 cm^{-1} can be observed for SnO₂ samples synthesized in H₂O and H₂O/MeOH medium. The absorption band with a maximum at 630 cm^{-1} is with higher intensity than the one with the maximum at 490 cm^{-1} in the FT-IR spectrums of SnO₂ synthesized in H₂O/EtOH and H₂O/iPrOH medium. In addition, next to the absorption band with the maximum at 630 cm^{-1} another absorption maximum at 670 cm^{-1} can be observed. The FT-IR spectrum is similar also in the case of SnO₂ synthesized in H₂O/Et.gl. media, only the most intense absorption of IR occurs at 670 instead of 630 cm^{-1} . Only single absorption band at 630 cm^{-1} can be observed for the sample synthesized in the H₂O/Glic. media.

Absorption band at 630 cm^{-1} is usually attributed to antisymmetric stretching vibrations of Sn-O-Sn near the material's surface while absorption band at ~ 670 and 490 cm^{-1} – to Sn-O stretching vibrations.

Great differences can be observed also in the recorded Raman spectrums of the samples (Fig. 8.b). The typical SnO₂ bands – E_g at 475 , A_{1g} at 632 and B_{2g} at 775 cm^{-1} can be observed in the recorded spectrums for all of the samples. The Raman spectrum of the samples synthesized in aqueous media and H₂O/MeOH additionally contains bands at 355 , 554 and 571 cm^{-1} . Raman band at 571 cm^{-1} are linked to the presence of amorphous tin hydroxide while the band at 554 cm^{-1} – to the surface defects of SnO₂ [7]. Raman bands below 400 cm^{-1} are usually inactive, however, in cases when material contains defects they can become active. Raman band at 355 cm^{-1} is linked to the Eu LO mode of SnO₂ [8]. Raman spectrum of the SnO₂ synthesized in H₂O/MeOH medium additionally contains bands at 1435 and 1460 cm^{-1} . Raman spectrums for the samples synthesized in the presence of EtOH, iPrOH or ethylene glycol greatly differs from the aforementioned cases. Raman bands at 554 and 571 cm^{-1} for the respective samples have lower intensities. Additionally, Raman bands at 355 and $\sim 1450\text{ cm}^{-1}$ was not detected for the respective samples, however, bands at 123 , 247 and 283 cm^{-1} can be observed. Rumyatseva *et.al.* have reported about the Raman bands in the respective region ($<300\text{ cm}^{-1}$), however, their causes are unclear and most likely could be related to activation of SnO₂ E_u mode due to various surface defects of SnO₂ [9]. The observed differences in the FT-IR and Raman spectrums (local structure) of the synthesized SnO₂ samples depending on the co-solvent used for their synthesis could be related to the gas sensing properties they show.

Thermal treatment in air at 673 K greatly affect gas sensitivity of the respective samples (Fig. 9).

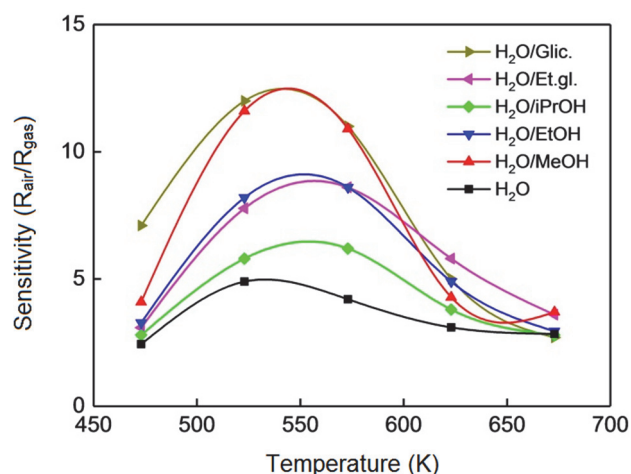


Fig.9. Ethanol (100 ppm) sensitivity of the hydrothermally synthesized SnO₂ after heat treatment at 673 K for 3h, depending on the medium used for SnO₂ synthesis.

After thermal treatment sensitivity of the samples decreases and the highest sensitivity (~12) at 523 K temperature shows the sample synthesized in the H₂O/MeOH and H₂O/Glic medium.

Substantial differences can be observed by comparing FT-IR and Raman spectrums of the samples before and after their thermal treatment at 673 K (Fig. 10). In FT-IR spectrums of the samples synthesized in H₂O/EtOH and H₂O/iPrOH media, similarly as in the case of the samples synthesized in H₂O and H₂O/MeOH media, only absorption bands at 630 and 490 cm⁻¹ can be observed after their thermal treatment. In the FT-IR spectrums of the samples synthesized in H₂O/Et.gl. and H₂O/Glic media a single absorption band at 630 cm⁻¹ can be observed after thermal treatment.

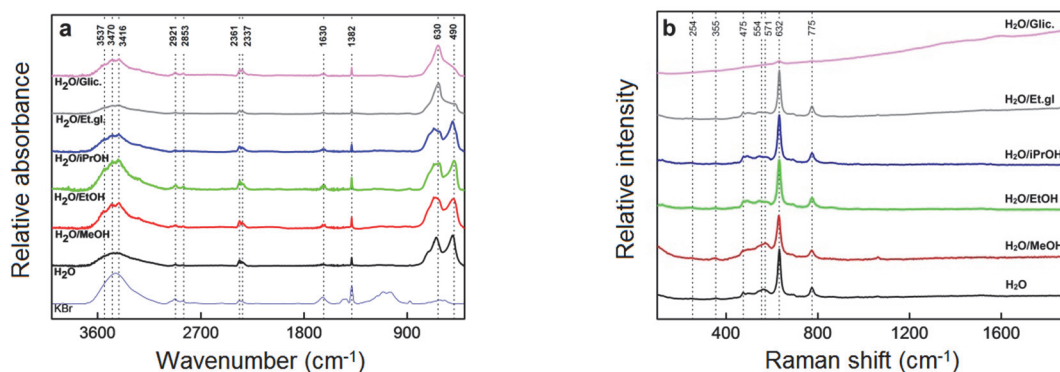


Fig.10. FT-IR (a) and Raman (b) spectrum of the hydrothermally synthesized SnO₂ after thermal treatment at 673 K for 3h, depending on the synthesis media used for the synthesis.

Typical SnO₂ Raman bands at 475, 632 and 775 cm⁻¹ dominates in the Raman spectrums of the thermally treated SnO₂ samples (Fig. 10. b). The observed differences in FT-IR and Raman spectrums of the samples after their thermal treatment indicates that thermal treatment affect local structure of the samples that can affect the gas sensing properties.

2.1. Obtaining of SnO₂ and Sb-doped SnO₂ ceramics by spark plasma sintering method, characterization of the obtained materials

Characterization of SnO₂ and Sb-doped SnO₂ prepared by co-precipitation method

All diffraction reflexes detected in the X-ray diffraction patterns (Fig. 11.) of the thermally treated solid products obtained by co-precipitation method were identified as corresponding to the cassiterite phase of SnO₂ (ICDD card No. 00-041-1445) independently of Sb content in the solid products. With an increase in the Sb content in the obtained materials, the full-width at half-maximum (FWHM) of the diffraction reflexes increases, indicating that the crystallite size decreases. Analogous correlation can be observed in the specific surface area (SSA) and calculated particle size of the compositions (table 4).

Increase in SSA and decrease in crystallite and particle size with an increase in the Sb content in the obtained Sn_{1-x}Sb_xO₂ compositions can be attributed increasing of Sb segregation in the surface layers of SnO₂ particles [10]. Sb³⁺ layer limits diffusion of Sn⁴⁺ ions from bulk to surface of the particles and limits their growth during the thermal treatment [11].

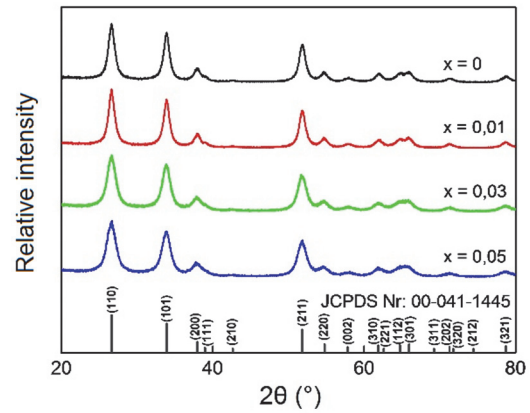


Fig. 11. X-ray diffraction patterns of the thermally treated (773 K) solid products obtained by co-precipitation method (x – nominal Sb concentration (mole %) in the composition with respect to Sn).

Table 4
SSA, average particle and crystallite size of the Sn_{1-x}Sb_xO₂ compositions obtained by thermal treatment (773 K) of the solid products obtained by co-precipitation method

Composition	SSA (m ² /g)	Average particle diameter (nm)	FWHM of diffraction reflex 110 ((°) 2θ)	Average crystallite size (nm)
SnO ₂	27.0	32	0,98	9.3
Sn _{0.99} Sb _{0.01} O ₂	27.5	31	1.00	9.1
Sn _{0.97} Sb _{0.03} O ₂	35.8	24	1.09	8.2
Sn _{0.95} Sb _{0.05} O ₂	44.1	20	1.36	6.5

The obtained Sn_{1-x}Sb_xO₂ compositions mainly consist of micron-sized agglomerates of nanoparticles (Fig. 12.).

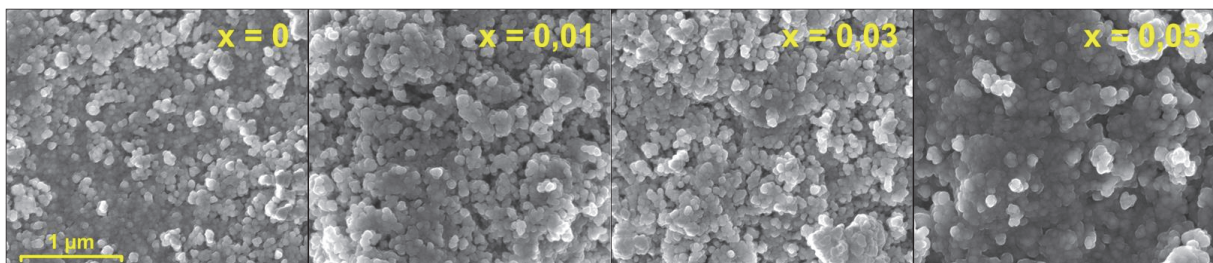


Fig. 12. SEM images of the surface morphology of the Sn_{1-x}Sb_xO₂ compositions obtained by thermal treatment (773 K) of the solid products obtained by co-precipitation method.

Sintering of SnO₂ and Sb-doped SnO₂ by spark plasma sintering method

Sn_{1-x}Sb_xO₂ powders were sintered at two different temperatures: 1223 and 1298 K (Fig. 13.). The *x*-axis of the graphs shows SPS process time, *y*₁-axis – temperature of the die, while *y*₂-axis – relative displacement of the pressing piston (provides information on the sample densification process during the SPS).

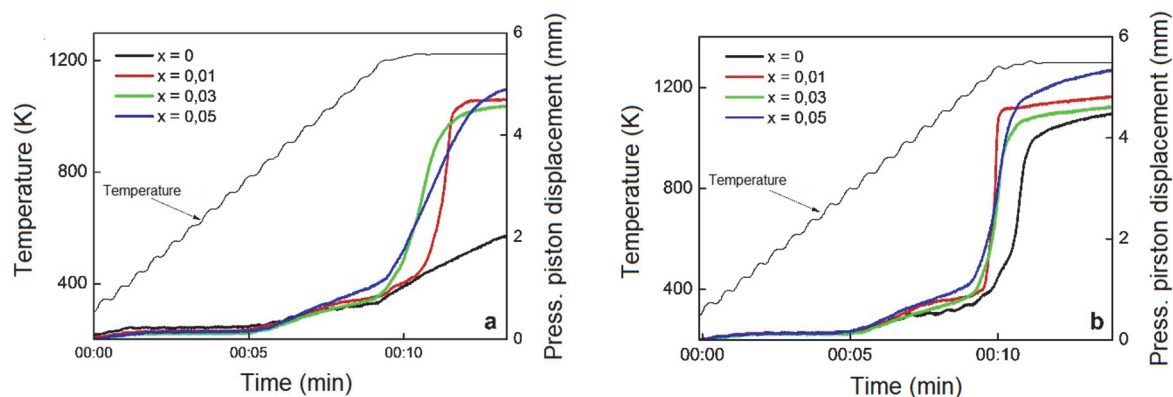


Fig.13. Graphical representation of the Sn_{1-x}Sb_xO₂ powders sintering process during the SPS, if sintering is done at 1223 K (a) and 1298 K (b) temperature.

The pressing piston displacement (Fig. 13.a) indicates that Sb doping lowers the sintering temperature of SnO₂ – the pressing piston for Sb-doped samples sintered at 1223 K has been moved ~2.5 mm further at the end of the sintering process compared to the SnO₂ sample. Additionally, it can be observed that sample's Sb content affect character of the piston displacement. Intensive densification also for the SnO₂ sample can be observed if the sintering is done at 1298 K temperature (Fig. 13.b), however, the most substantial pressing piston movement for the SnO₂ sample occurs at higher temperature (1240–1298 K) than for the Sb-doped samples (1223–1285 K) sintered at the respective temperature.

Since antimony depending on the oxidation state (Sb³⁺ or Sb⁵⁺) in which it incorporates into the lattice of SnO₂ can increase the number of oxygen or tin vacancies in the oxide the increased amount of cation and anion vacancies can enhance mass transfer and improve the densification of SnO₂ during the SPS.

Characterization of the spark plasma sintered Sn_{1-x}Sb_xO₂ samples

All of the detected diffraction reflexes in the diffraction patterns of the Sn_{1-x}Sb_xO₂ samples sintered at 1223 K (Fig. 14.a) were identified as corresponding to the cassiterite phase of SnO₂ independently of the sample's Sb content. For the samples sintered at 1298 K temperature additionally a presence of Sb₂O₃ (ICDD card No. 00-011-0691) phase was detected in the case of Sn_{0.95}Sb_{0.05}O₂ composition sample (Fig. 14.b.). Most likely the reducing conditions during SPS at high temperatures promotes reduction of Sb⁵⁺ to Sb³⁺ and formation of Sb₂O₃ phase when Sb³⁺ reaches the solubility limit in SnO₂.

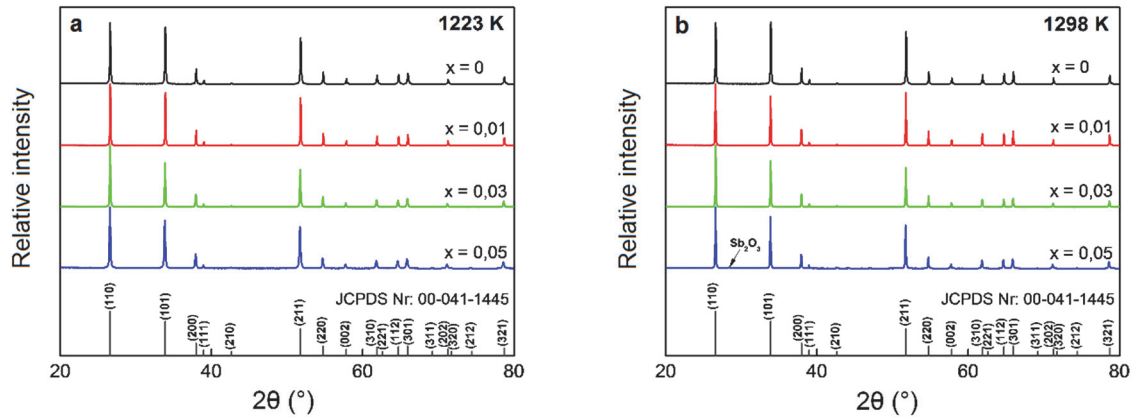


Fig. 14. X-ray diffraction patterns of the $\text{Sn}_{1-x}\text{Sb}_x\text{O}_2$ samples obtained by SPS at 1223 (a) and 1298 K (b) temperature.

The lattice parameters of SnO_2 increases with increasing Sb content in the sintered samples (table 5) indicating that Sb ions are incorporated into the SnO_2 lattice. The sintering temperature does not significantly affect lattice parameters of the samples. Since ionic radius of Sb^{3+} (0.76 Å) is larger than of Sb^{5+} (0.60 Å) and Sn^{4+} (0.69 Å) the increase in SnO_2 lattice parameters with Sb doping indicates that antimony into the SnO_2 lattice mainly incorporates as Sb^{3+} , that is also testified by the detected presence of Sb_2O_3 phase in the case of the $\text{Sn}_{0.95}\text{Sb}_{0.05}\text{O}_2$ composition sample sintered at 1298 K temperature.

Table 5
Identified phases and lattice parameters (SnO_2 phase) of the $\text{Sn}_{1-x}\text{Sb}_x\text{O}_2$ samples obtained by SPS at 1223 and 1298 K temperature

Sample composition	Lattica constant (Å)		Unit cell volume (Å ³)	Identified phases
	$a = b$	c		
SnO_2 (1223K)	4.738	3.187	71.55	SnO_2
$\text{Sn}_{0.99}\text{Sb}_{0.01}\text{O}_2$ (1223K)	4.739	3.187	71.56	SnO_2
$\text{Sn}_{0.97}\text{Sb}_{0.03}\text{O}_2$ (1223K)	4.741	3.190	71.70	SnO_2
$\text{Sn}_{0.95}\text{Sb}_{0.05}\text{O}_2$ (1223K)	4.744	3.193	71.83	SnO_2
SnO_2 (1298K)	4.738	3.187	71.56	SnO_2
$\text{Sn}_{0.99}\text{Sb}_{0.01}\text{O}_2$ (1298K)	4.738	3.187	71.56	SnO_2
$\text{Sn}_{0.97}\text{Sb}_{0.03}\text{O}_2$ (1298K)	4.741	3.190	71.71	SnO_2
$\text{Sn}_{0.95}\text{Sb}_{0.05}\text{O}_2$ (1298K)	4.744	3.193	71.84	$\text{SnO}_2 + \text{Sb}_2\text{O}_3$

Both sintering temperature and Sb content greatly affect microstructure of the SPSed samples (see Fig. 15.). Microstructure of the SnO_2 sample sintered at 1223 K temperature is inhomogeneous. It mainly consist of grains with size <100 nm, however, also presence of comparatively large grains with size in the range of 1–15 μm can be observed in the sample. Microstructure of the $\text{Sn}_{0.99}\text{Sb}_{0.01}\text{O}_2$ composition sample sintered at 1223 K is also inhomogeneous and consist of both nanosized (280–600 nm) and micronsized (1–8 μm) grains. Since the $\text{Sn}_{1-x}\text{Sb}_x\text{O}_2$ powders used for the SPS mainly consists of micron-sized agglomerates of nanoparticles (Fig. 12.), an important role in the formation of inhomogeneous microstructure of the sintered samples could play an uneven density distribution of the sinterable powder in the sintering die [12]. Microstructure of the $\text{Sn}_{0.97}\text{Sb}_{0.03}\text{O}_2$ and $\text{Sn}_{0.95}\text{Sb}_{0.05}\text{O}_2$ composition samples are relatively homogeneous and mainly consists of grains with size <300 nm. As can be expected, grain size for all $\text{Sn}_{1-x}\text{Sb}_x\text{O}_2$ samples sintered at 1298 K is larger than that of the ones sintered at 1223 K temperature. Microstructure of the SnO_2 sample sintered at 1298 K mainly consist of micron sized (0.7–3 μm) grains, however, also regions with nanosized (80–250 nm) grains can be observed in the sample. Bimodal grain size distribution is characteristic

also for the $\text{Sn}_{0.99}\text{Sn}_{0.01}\text{O}_2$ composition sample sintered at 1298 K – although it mainly consists of grains with size in the range of 0.6–1.5 μm , the presence of substantially larger grains with size $>3 \mu\text{m}$ can be observed in the sample as well. The $\text{Sn}_{0.97}\text{Sb}_{0.03}\text{O}_2$ composition sample sintered at 1298 K temperature consist of grains with size in the range of 0.5–2.2 μm , while the $\text{Sn}_{0.95}\text{Sb}_{0.05}\text{O}_2$ composition sample – of grains with size in the range of 50 to 270 nm. Microstructural homogeneity of both at 1223 and 1298 K temperature sintered Sb containing $\text{Sn}_{1-x}\text{Sb}_x\text{O}_2$ samples increases with increase in their Sb content. This, similarly as in the case of the synthesized $\text{Sn}_{1-x}\text{Sb}_x\text{O}_2$ powders, can be attributed to Sb^{3+} segregation in the surface layers of SnO_2 grains.

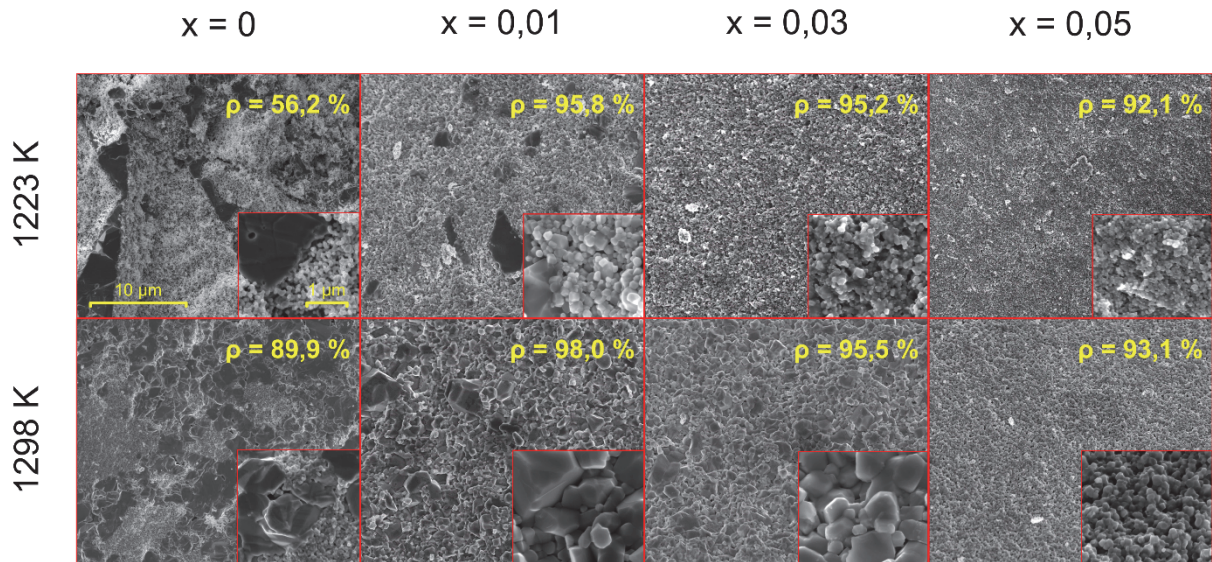


Fig. 15. Fracture surfaces (SEM) of the $\text{Sn}_{1-x}\text{Sb}_x\text{O}_2$ samples obtained by SPS at 1223 (a) and 1298 K (b) temperature.

Relative density of both at 1223 and 1298 K temperature sintered Sb containing samples exceeds 90 %. The density of SnO_2 samples, as it was indicated by the pressing piston displacement (Fig. 13.), increases from 56.2 to 89.9 % (of theoretical density), if sintering temperature is increased from 1223 to 1298 K.

Both sintering temperature and Sb-content greatly affect the electrical conductivity of the SPSed samples (see Fig. 16.).

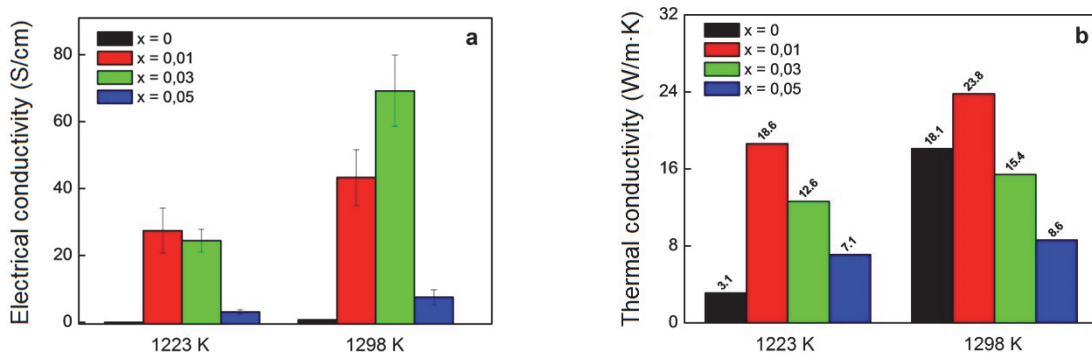


Fig. 16. Electrical (a) and thermal conductivity (b) at room temperature of the $\text{Sn}_{1-x}\text{Sb}_x\text{O}_2$ samples obtained by SPS at 1223 and 1298 K temperature.

Electrical conductivity of the Sb-containing samples obtained at both sintering temperatures are higher than that of the SnO_2 samples, however, it strongly depends on their Sb content. The highest electrical conductivity ($\sim 27 \text{ S/cm}$) of all samples sintered at 1223 K have the sample

with the composition of $\text{Sn}_{0.99}\text{Sb}_{0.01}\text{O}_2$, while for the samples with higher Sb content electrical conductivity decreases with increase in their Sb content. With increase in sintering temperature electrical conductivity of all samples increases. The electrical conductivity of the Sb-containing samples sintered at 1298 K temperature increases until Sb content in the samples nominally reaches 3 mol % (~69 S/cm) and then considerably decreases for the 5 mol % Sb-doped sample. The observed changes in electrical conductivity of the Sb-containing samples depending on their Sb content can be attributed to the presence of both Sb oxidation states (Sb^{3+} and Sb^{5+}) as well as to the microstructure of the samples. Shallow donor levels close to the conduction band of SnO_2 forms if Sb^{5+} is electronically compensated and as a result SnO_2 exhibits high *n*-type conductivity already at room temperature. Sb^{3+} in the SnO_2 lattice can be compensated both ionically and electronically, however, since *p*-type conductivity in SnO_2 is difficult to achieve, ionic compensation is considered as the dominant compensation mechanism. Although the increase of SnO_2 lattice parameters with Sb doping (Table 5) indicates that antimony mainly incorporates into the lattice of $\text{Sn}_{1-x}\text{Sb}_x\text{O}_2$ samples as Sb^{3+} , their relatively high electrical conductivity with respect to the SnO_2 samples is attributable to the electronic compensation mechanism of Sb^{5+} . Possibly, electronic compensation mechanism of Sb^{3+} starts to play a substantial role in the case of 5 mol % Sb-doping, causing a decrease in the electrical conductivity of the respective samples, since with an increase in Sb content the ratio between $\text{Sb}^{3+}/\text{Sb}^{5+}$ ions incorporated into the lattice of SnO_2 increases [13]. Comparatively smaller grain size of the $\text{Sn}_{0.97}\text{Sb}_{0.03}\text{O}_2$ composition sample sintered at 1223 K could be the main reason why its conductivity is lower than that of the $\text{Sn}_{0.99}\text{Sb}_{0.01}\text{O}_2$ composition sample sintered at the respective temperature. The increase in grain size and density of the samples (Fig. 15.) are the main reasons why electrical conductivity of the $\text{Sn}_{1-x}\text{Sb}_x\text{O}_2$ samples sintered at 1298 K temperature is higher than that of the ones sintered at 1223 K temperature.

The thermal conductivity of all Sb-containing samples sintered at 1223 K temperature is higher than the one of SnO_2 sample (related to the relatively low density of the sample (Fig. 15.)) sintered at the respective temperature, however, it decreases with increase in their Sb content. Since atomic mass and radius of Sb and Sn are quite similar, the observed decrease in thermal conductivity with increase in their Sb content is attributable to the microstructural differences of the samples (Fig. 15.). Similarly, as in the case of electrical conductivity, the thermal conductivity of all samples increases with increase in sintering temperature. Thermal conductivity of the SnO_2 sample sintered at 1223 K temperature is lower only than $\text{Sn}_{0.99}\text{Sb}_{0.01}\text{O}_2$ composition sample sintered at the respective temperature while higher than the samples with composition of $\text{Sn}_{0.99}\text{Sb}_{0.01}\text{O}_2$ and $\text{Sn}_{0.97}\text{Sb}_{0.03}\text{O}_2$. The substantially increased thermal conductivity of the SnO_2 sample sintered at 1298 K temperature (18.1 W/m·K) compared to the one sintered at 1223 K temperature (3.1 W/m·K) is attributable to its considerably higher density and larger grain size (Fig. 15.). Similarly as in the case of the Sb-doped samples sintered at 1223 K temperature, the thermal conductivity of the Sb-containing samples sintered at 1298 K temperature decreases with increase in their Sb content. Microstructural differences (smaller grain size) is the main reason for the lower thermal conductivity of the $\text{Sn}_{0.97}\text{Sb}_{0.03}\text{O}_2$ un $\text{Sn}_{0.95}\text{Sb}_{0.05}\text{O}_2$ composition samples sintered at 1298 K temperature compared to the SnO_2 sample sintered at the respective temperature despite to their higher densities.

Characterization of the post-spark plasma sintering annealed $\text{Sn}_{1-x}\text{Sb}_x\text{O}_2$ samples

Annealing under air was done for the samples sintered at 1298 K temperature.

Electrical conductivity (Fig. 17.) for all Sb-containing samples greatly increases after annealing independently of the annealing temperature, while for the SnO₂ sample decreases (from ~0.7 S/cm for the unannealed sample to ~0.02 S/cm for the sample annealed at 1248 K temperature). Similarly as in the case of the Sb-containing samples sintered at 1298 K temperature, the electrical conductivity of the post-SPS annealed Sb-containing samples increases till Sb content in the samples nominally reaches 3 mol % and then considerably decreases for the 5 mol % doped sample.

Atmospheric oxygen can fill the oxygen vacancies of SnO₂ during the annealing process, attracting electrons that were liberated into the during the vacancy formation. As a result, the electrical conductivity of the annealed SnO₂ samples decreases as compared to the unannealed one. In the case of Sb containing samples, annealing can cause oxidation of Sb³⁺ ions present into the lattice of SnO₂ to Sb⁵⁺. As a result, more electrons are liberated into the conduction band of SnO₂ and conductivity of the samples increases. Electrical conductivity of the samples increases till annealing temperature of 1173 K is reached, indicating that the equilibrium ratio between the Sb³⁺ and Sb⁵⁺ states into the oxide is reached.

About the oxidation of Sb³⁺ to Sb⁵⁺ during the annealing of the Sb containing samples indicates the detected presence of Sb₂O₄ phase in the case of the Sn_{0.95}Sb_{0.05}O₂ composition sample (after sintering the presence of the Sb₂O₃ phase was detected in the respective sample (see Fig. 14.)), the decrease in lattice parameters of all annealed samples in comparison to the unannealed ones (Table 6) as well as the shift of the Sb 3d_{3/2} peak in the XPS spectrums of the annealed Sb containing samples towards higher binding energy.

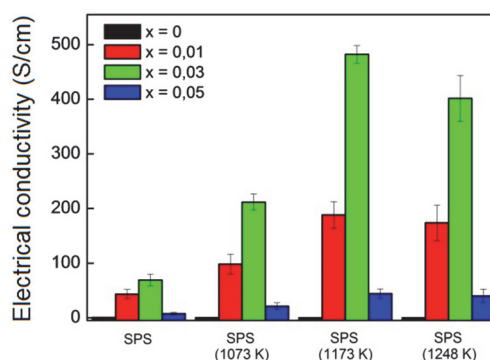


Fig. 17. Electrical conductivity of the Sn_{1-x}Sb_xO₂ samples obtained by SPS at 1298 K after annealing under air.

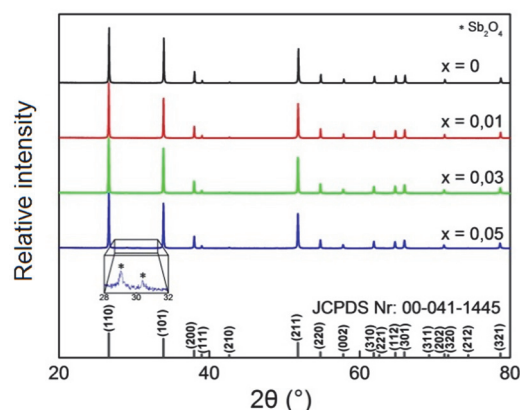


Fig.18. X-ray diffraction patterns of the Sn_{1-x}Sb_xO₂ samples obtained by SPS at 1298 K after annealing under air at 1173 K.

Table 6
Identified phases and lattice parameters (SnO₂ phase) of the Sn_{1-x}Sb_xO₂ samples obtained by SPS at 1298 K temperature before and after annealing at 1173 K under air

Sample composition (sintering/annealing temperature)	Lattice constant (Å)		Unit cell volume (Å ³)	Identified phases
	<i>a</i> = <i>b</i>	<i>c</i>		
SnO ₂ (1298 K/–)	4.738	3.187	71.56	SnO ₂
Sn _{0.99} Sb _{0.01} O ₂ (1298K/–)	4.738	3.187	71.56	SnO ₂
Sn _{0.97} Sb _{0.03} O ₂ (1298 K/–)	4.741	3.190	71.71	SnO ₂
Sn _{0.95} Sb _{0.05} O ₂ (1298 K/–)	4.744	3.193	71.84	SnO ₂ + Sb ₂ O ₃
SnO ₂ (1298K/1173 K)	4.738	3.187	71.56	SnO ₂
Sn _{0.99} Sb _{0.01} O ₂ (1298 K/1173 K)	4.738	3.187	71.56	SnO ₂
Sn _{0.97} Sb _{0.03} O ₂ (1298 K/1173 K)	4.740	3.190	71.69	SnO ₂
Sn _{0.95} Sb _{0.05} O ₂ (1298 K/1173 K)	4.742	3.191	71.75	SnO ₂ + Sb ₂ O ₄

Annealing affects not only electrical conductivity but Seebeck coefficient and thermal conductivity of the samples as well (see Table 7). Seebeck coefficient for both the annealed and unannealed samples is negative (*n*-type conductivity). Since Seebeck coefficient and electrical conductivity (charge carrier concentration) are inversely proportional, the increase in Seebeck coefficient of the annealed SnO₂ sample as compared to the unannealed one is related to decrease in its conductivity. Seebeck coefficient of the Sb-containing samples decreases after annealing. Although electrical conductivity of both the annealed and unannealed Sn_{0.95}Sb_{0.05}O₂ composition sample is lower than that of the annealed and unannealed sample with composition of Sn_{0.97}Sb_{0.03}O₂, the Seebeck coefficient of the Sn_{0.95}Sb_{0.05}O₂ composition sample is lower. As discussed above, possibly, when Sb³⁺ in SnO₂ reaches a certain concentration, electronic compensation mechanism of Sb³⁺ starts to play a greater role, thus compensating the contribution of Sb⁵⁺ to electrical conductivity and Seebeck coefficient of the samples. The thermal conductivity of the samples after annealing increases (4–15 %, depending on the sample Sb content), that can be attributed to the decrease in lattice defects and increase in electrical conductivity of the samples (Sb-doped ones). The increase in electrical conductivity due to annealing of the Sb-doped samples compensates the decrease in their Seebeck coefficient and improves their thermoelectric power factor.

Table 7

Electrical conductivity, Seebeck coefficient, thermal conductivity and thermoelectric power factor near room temperature of the Sn_{1-x}Sb_xO₂ samples obtained by SPS at 1298 K temperature before and after annealing at 1173 K under air

Sample composition (sintering/annealing temperature)	Electrical conductivity (S/cm)	Seebeck coefficient (μ V/K)	Thermal conductivity (W/m·K)	Thermoelectric power factor (mW/m·K ²)
SnO ₂ (1298 K/-)	0.73	-224.3	18.9	0.0036
Sn _{0.99} Sb _{0.01} O ₂ (1298 K/-)	43.3	-73.4	23.8	0.0233
Sn _{0.97} Sb _{0.03} O ₂ (1298 K/-)	69.2	-27.4	15.4	0.0054
Sn _{0.95} Sb _{0.05} O ₂ (1298 K/-)	7.6	-24.7	8.6	0.0005
SnO ₂ (1298K/1173 K)	0.03	-261.8	20.1	0.0002
Sn _{0.99} Sb _{0.01} O ₂ (1298 K/1173 K)	188.3	-61.2	24.6	0.0705
Sn _{0.97} Sb _{0.03} O ₂ (1298 K/1173 K)	482.1	-21.9	18.3	0.0231
Sn _{0.95} Sb _{0.05} O ₂ (1298 K/1173 K)	44.3	-21.6	10.2	0.0020

The electrical conductivity of the SnO₂ sample annealed at 1173 K increases with increase in temperature (Fig. 19.a), indicating the semiconducting behavior of SnO₂. Electrical conductivity of all Sb-containing samples initially decreases with increase in temperature, however, when temperature of ~650–700 K is reached it starts to increase, particularly in the case of the Sn_{0.97}Sb_{0.03}O₂ composition sample. Similar observations have been made in some other studies of Sb-containing ceramics and glasses, where the change in electrical conductivity of the characterised samples with increase in temperature is attributed to fluctuations between Sb³⁺ and Sb⁵⁺ states due to influence of the temperature [14], [15].

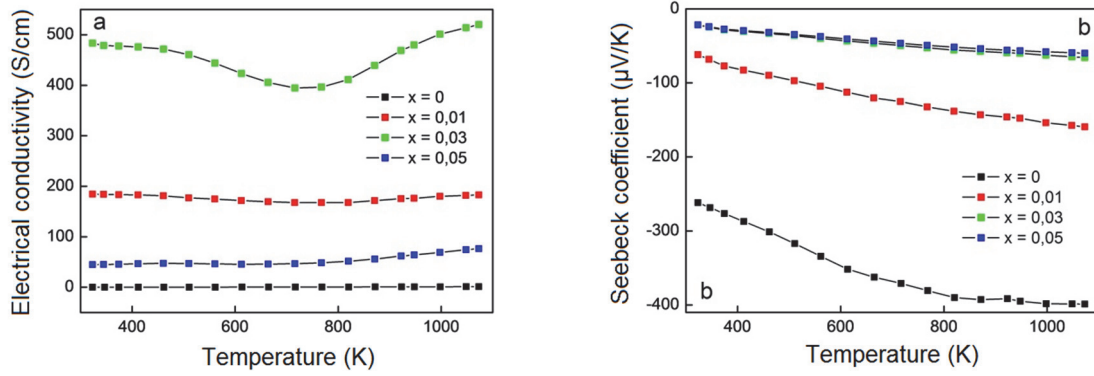


Fig. 19. Electrical conductivity (a) and Seebeck coefficient (b) of the post-SPS (1298 K) annealed (1173 K under air) $\text{Sn}_{1-x}\text{Sb}_x\text{O}_2$ samples as a function of temperature (323–1073 K).

Seebeck coefficient for all $\text{Sn}_{1-x}\text{Sb}_x\text{O}_2$ composition samples annealed at 1173 K increases with increase in temperature (Fig. 19.b). The highest value of Seebeck coefficient ($\sim 400 \mu\text{V/K}$) at 1073 K temperature has the SnO_2 sample. The highest Seebeck coefficient at 1073 K among the Sb containing samples have the sample with composition of $\text{Sn}_{0.99}\text{Sb}_{0.01}\text{O}_2$ ($\sim 159 \mu\text{V/K}$).

Although Seebeck coefficient of the Sb containing samples is several times lower than the one of the SnO_2 sample, the thermoelectric power factor for all of the Sb containing samples is higher due to compensation by their relatively higher electrical conductivity (Fig. 20.). The highest value of thermoelectric power factor ($\sim 0.46 \text{ mW/m}\cdot\text{K}^2$) at 1073 K temperature shows the sample with composition of $\text{Sn}_{0.99}\text{Sb}_{0.01}\text{O}_2$. Although the highest electrical conductivity have the sample with composition of $\text{Sn}_{0.97}\text{Sb}_{0.03}\text{O}_2$, due to the substantially lower Seebeck coefficient (Fig. 19.b) its thermoelectric power factor is lower than the one of the $\text{Sn}_{0.99}\text{Sb}_{0.01}\text{O}_2$ composition sample decreases its value of thermoelectric power factor.

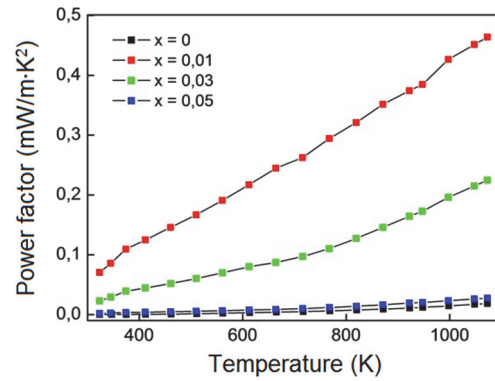


Fig. 20. Thermoelectric power factor of the post-SPS (1298 K) annealed (1173 K under air) $\text{Sn}_{1-x}\text{Sb}_x\text{O}_2$ samples as a function of temperature (323–1073 K).

Thermal conductivity for all samples annealed at 1173 K, except that of the $\text{Sn}_{0.97}\text{Sb}_{0.03}\text{O}_2$ composition, decreases in a similar trend with increase in temperature (Fig. 21.a). Thermal conductivity of the $\text{Sn}_{0.97}\text{Sb}_{0.03}\text{O}_2$ composition sample decreases slower and at 1073 K shows the highest thermal conductivity ($\sim 8 \text{ W/m}\cdot\text{K}$) among all the samples. Although at room temperature the thermal conductivity of the samples depending on their Sb content differs even 2.4 times (samples with composition of $\text{Sn}_{0.99}\text{Sb}_{0.01}\text{O}_2$ and $\text{Sn}_{0.95}\text{Sb}_{0.05}\text{O}_2$), at 1073 K the difference does not exceed 1.2 times. This can be explained by a change in the mechanisms controlling the thermal conductivity. While at room temperature the dominant mechanism that affects thermal conductivity of the material is the boundary and point-defect scattering, at high temperatures Umklapp scattering becomes the dominant mechanism. The main reason why thermal conductivity of the $\text{Sn}_{0.97}\text{Sb}_{0.03}\text{O}_2$ composition sample decreases slower with increase in temperature as compared to the other samples is its comparably higher electrical conductivity (Fig. 19.a).

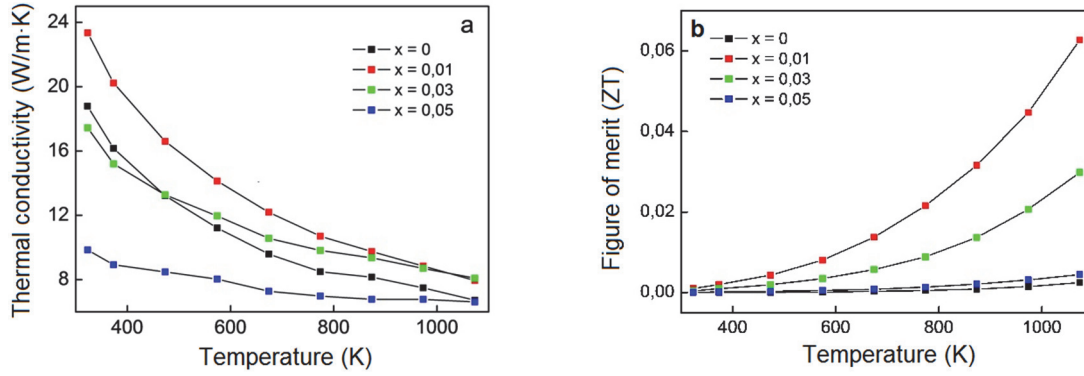


Fig.21. Thermal conductivity (a) and thermoelectric figure of merit (b) of the post-SPS (1298 K) annealed (1173 K under air) Sn_{1-x}Sb_xO₂ samples as a function of temperature (323–1073 K).

Thermoelectric figure of merit for all Sn_{1-x}Sb_xO₂ samples annealed at 1173 K temperature increases with increase in temperature (Fig. 21.b). The thermoelectric figure of merit for all Sb-containing samples is higher than that if the SnO₂ sample at all temperatures that results from their electrical conductivity, Seebeck coefficient and thermal conductivity values. The highest figure of merit (~0.06) at 1073 K temperature shows the sample with composition of Sn_{0.99}Sb_{0.01}O₂.

The values of the electrical conductivity (σ), Seebeck coefficient (S), thermal conductivity (k), thermoelectric power factor (PF) and thermoelectric figure of merit (ZT) of the post-SPS (1298 K) annealed (1173 K under air) Sn_{1-x}Sb_xO₂ samples at 1073 K temperature can be seen in Table 8.

Table 8

Thermoelectric properties of the post-SPS (1298 K) annealed (1173 K under air) Sn_{1-x}Sb_xO₂ samples at 1073 K temperature

Sample composition	σ (S/cm)	S (μ V/K)	k (W/m \times K)	k_{el} (W/m \times K)	k_{kr} (W/m \times K)	PF (mW/m \times K ²)	ZT
SnO ₂	1.19	398.9	6.72	0.003	6.718	0.02	0.002
Sn _{0.99} Sb _{0.01} O ₂	182.8	159.3	7.94	0.480	7.464	0.46	0.062
Sn _{0.97} Sb _{0.03} O ₂	520.3	65.7	8.08	1.368	6.718	0.22	0.029
Sn _{0.95} Sb _{0.05} O ₂	76.6	59.9	6.61	0.201	6.415	0.03	0.004

CONCLUSIONS

1. The amount of HCl or NaOH added to the hydrothermal synthesis starting solution affect crystallite size, specific surface area, morphology and gas sensing properties of the synthesized SnO₂;
2. The addition of co-solvent (alcohol), as well its type (methanol, ethanol, isopropanol, ethyleneglycol, glycerol) affect crystallite size, local structure, specific surface area, morphology and gas sensing properties of the hydrothermally synthesized SnO₂;
3. Sb-doping (1–5 mole %) reduces crystallite size and increases specific surface area of the SnO₂ obtained by chemical co-precipitation method;
4. Sb-doping (1–5 mole %) reduces sintering temperature of SnO₂, if sintering is done by spark plasma sintering method, and allows to obtain dense samples (relative density >90 %) at 75 K degrees lower temperature (1223 K) than in the case of undoped SnO₂ (1298 K);
5. Sb-doping (1–5 mole %) enhances electrical conductivity of SnO₂ ceramics obtained by spark plasma sintering method, however, it strongly depends on sintering temperature and Sb content in the samples;
6. Annealing under air enhances electrical conductivity of Sb doped SnO₂ ceramics obtained by spark plasma sintering method and as improves its thermoelectric power factor.
7. The highest value of thermoelectric figure of merit of Sb (1–5 mole %) doped SnO₂ ceramic is obtained at sample composition of Sn_{0.99}Sb_{0.01}O₂.

LITERATURE REFERENCES

- [1] Q. Zhao, L. Ma, Q. Zhang, C. Wang, X. Xu, SnO₂-Based Nanomaterials: Synthesis and Application in Lithium-Ion Batteries and Supercapacitors, *J. Nanomater.*, 2015, 2015, Article ID 850147;
- [2] T. Tsubota, S. Kobayashi, N. Murakami, T. Ohno, Improvement of Thermoelectric Performance for Sb-Doped SnO₂ Ceramics Material by Addition of Cu as Sintering Additive, *J. Electron. Mater.*, 43, 2014, pp. 3567–3573;
- [3] S. Yanagiya, N. V. Nong, J. Xu, M. Sonne, N. Pryds, Thermoelectric Properties of SnO₂ Ceramics Doped with Sb and Zn, *J. Electron. Mater.*, 40, 2011, pp. 674–677;
- [4] L. Wang, L. Zhuo, Y. Yu, F. Zhao, High-rate performance of SnS₂ nanoplates without carbon-coating as anode material for lithium ion batteries, *Electrochim. Acta.*, 112, 2013, pp. 439–447;
- [5] C. Wang, L. Yin, L. Zhang, D. Xiang, R. Gao, Metal Oxide Gas Sensors: Sensitivity and Influencing Factors, *Sensors.*, 10, 2010, pp. 2088–2106;
- [6] M. Batzill, Surface Science Studies of Gas Sensing Materials: SnO₂, *Sensors*, 6(10), 2006, pp. 1345–1366;
- [7] M. Ristić, M. Ivanda, S. Popović, S. Musić, Dependence of nanocrystalline SnO₂ particle size on synthesis route, *J. Non. Cryst. Solids.*, 303, 2002, pp. 270–280;
- [8] O. Lupan, L. Chow, G. Chai, A. Schulte, S. Park, H. Heinrich, A rapid hydrothermal synthesis of rutile SnO₂ nanowires, *Mater. Sci. Eng. B Solid-State Mater. Adv. Technol.*, 157, 2009, pp. 101–104;
- [9] M. N. Rumyantseva, A. M. Gaskov, N. Rosman, T. Pagnier, J. R. Morante, Raman surface vibration modes in nanocrystalline SnO₂: correlation with gas sensing performances, *Chem. Mater.*, 17, 2005, pp. 893–901;
- [10] D. R. Leite, I. O. Mazali, E. C. Aguiar, W. C. Las, M. Cilense, The effect of Sb and Nb on the electrical conductivity of tin dioxide based ceramics, *J. Mater. Sci.*, 41, 2006, pp. 6256–6259;
- [11] Y.-Q. Li, J.-L. Wang, S.-Y. Fu, S.-G. Mei, J.-M. Zhang, K. Yong, Facile synthesis of antimony-doped tin oxide nanoparticles by a polymer-pyrolysis method, *Mater. Res. Bull.*, 45, 2010, pp. 677–681;
- [12] C. D. Sagel-Ransijn, a. J. a. Winnubst, B. Kerkwijk, a. J. Burggraaf, H. Verweij, Production of defect-poor nanostructured ceramics of Yttria-Zirconia, *J. Eur. Ceram. Soc.*, 17, 1997, pp. 831–841;
- [13] C. Terrier, J. Chatelon, R. Berjoan, J. Roger, Sb-doped SnO₂ transparent conducting oxide from the sol-gel dip-coating technique, *Thin Solid Films.*, 263, 1995, pp. 37–41;
- [14] M. L. Arefin, F. Raether, D. Dolejš, A. Klimera, Phase formation during liquid phase sintering of ZnO ceramics, *Ceram. Int.*, 35, 2009, pp. 3313–3320;
- [15] P. Brahma, S. Banerjee, S. Chakraborty, D. Chakravorty, Small polaron and bipolaron transport in antimony oxide doped barium hexaferrites, *J. Appl. Phys.*, 88, 2000, 6526.

AUTHOR'S PUBLICATIONS AND PARTICIPATION IN CONFERENCES

Scientific articles (relevant to the dissertation):

1. K. Rubenis, S. Populoh, P. Thiel, S. Yoon, U. Müller, J. Locs. Thermoelectric properties of dense Sb-doped SnO₂ ceramics. *Journal of Alloys and Compounds*, 2017, Vol. 692, pp. 515–521. (Available in Scopus database);
2. K. Rubenis, J. Locs. Hydrothermal synthesis of SnO₂ structures with various morphologies in the presence of different alcoholic co-solvents. *Key Engineering Materials*, 2017, Vol. 721, pp. 87–91. (Available in Scopus database);
3. K. Rubenis, J. Locs, J. Mironova, R. Merijs-Meri. Influence of phase separation on thermal conductivity of Ti_{1-x}Sb_xO₂ ceramics. *Journal of Ceramic Science and Technology*, 2016, Vol. 7(1), pp. 135–138. (Available in Scopus database);

Scientific articles (not relevant to the dissertation):

4. P. Thiel, S. Populoh, S. Yoon, G. Saucke, K. Rubenis, A. Weidenkaff. Charge-carrier hopping in highly conductive CaMn_{1-x}M_xO_{3-δ}. *The Journal of Physical Chemistry C*, 2015, Vol. 119(38), pp. 21860–21867. (Available in Scopus database);
5. K. Rubenis, A. Pura, V. Teteris, J. Locs, J. Ozolins. Effect of shaping method and heat treatment on microstructure and thermoelectric properties of titanium dioxide. *Key Engineering Materials*, 2014, Vol. 604, pp. 240–244. (Available in Scopus database).

Scientific conferences:

1. K. Rubenis, J. Locs. Hydro/Solvothermal synthesis of various SnO₂ nano/microstructures. *COST – TO-BE Spring Meeting 2017*, Luksemburga, Luksemburga, 3–5. aprīlis, 2017;
2. K. Rubenis, J. Locs, S. Populoh. “Thermoelectric properties of Sb doped SnO₂ ceramics”. *Electronic Materials and Applications 2017*, Orlando, ASV, 18–20. janvāris, 2017;
3. K. Rubenis, J. Locs. Hydrothermal synthesis of SnO₂ structures with various morphologies in the presence of different alcoholic co-solvents. *BALTMATTRIB 2016: The 25th International Conference of Engineering Materials & Tribology*, Rīga, Latvija, 3–4. novembris, 2016;
4. K. Rubenis, J. Ločs. Ar dzirksteļizlādes plazmas saķepināšanas metodi iegūtas Sb aizvietotas SnO₂ keramikas termoelektriskās īpašības. *LU Cietvielu fizikas institūta 32. zinātniskā konference*, Rīga, Latvija, 17–19. februāris, 2016;
5. J. Locs, K. Rubenis. Thermoelectric properties of TiO₂ based materials. *CIMTEC 2014: 13th International Conference on Modern Materials and Technologies*, Montekatīni – Terme, Toskāna, Itālija, 8–20 jūnijs, 2014;
6. K. Rubenis, J. Ločs, L. Bērziņa-Cimdiņa. Uz TiO₂ bāzētu materiālu sintēze ar sola-gēla metodi. *LU Cietvielu fizikas institūta 30. zinātniskā konference*. Rīga, Latvija, 19–21. februāris, 2016;
7. K. Rubenis, A. Pura, V. Teteris, J. Locs, J. Ozolins. Effect of shaping method and heat treatment on microstructure and thermoelectric properties of titanium dioxide. *BALTMATTRIB 2013: The 22nd International Conference of Engineering Materials & Tribology*, Rīga, Latvija, 14–15. novembris, 2013;
8. K. Rubenis, J. Locs, V. Teteris, J. Barloti, L. Berzina-Cimdina. Thermoelectric properties of nonstoichiometric titanium dioxide formed by die pressing and extrusion. Shaping 5: 5th International Conference on Shaping of Advanced Ceramics, Monsa, Beļģija, 29–31. janvāris, 2013.